NANO LETTERS

Subscriber access provided by GAZI UNIV

Communication

Impacts of Ion Segregation on Local Optical Properties in Mixed Halide Perovskite Films

Olivia Hentz, Zhibo Zhao, and Silvija Gradecak

Nano Lett., **Just Accepted Manuscript** • DOI: 10.1021/acs.nanolett.5b05181 • Publication Date (Web): 13 Jan 2016

Downloaded from http://pubs.acs.org on January 19, 2016

Just Accepted

"Just Accepted" manuscripts have been peer-reviewed and accepted for publication. They are posted online prior to technical editing, formatting for publication and author proofing. The American Chemical Society provides "Just Accepted" as a free service to the research community to expedite the dissemination of scientific material as soon as possible after acceptance. "Just Accepted" manuscripts appear in full in PDF format accompanied by an HTML abstract. "Just Accepted" manuscripts have been fully peer reviewed, but should not be considered the official version of record. They are accessible to all readers and citable by the Digital Object Identifier (DOI®). "Just Accepted" is an optional service offered to authors. Therefore, the "Just Accepted" Web site may not include all articles that will be published in the journal. After a manuscript is technically edited and formatted, it will be removed from the "Just Accepted" Web site and published as an ASAP article. Note that technical editing may introduce minor changes to the manuscript text and/or graphics which could affect content, and all legal disclaimers and ethical guidelines that apply to the journal pertain. ACS cannot be held responsible for errors or consequences arising from the use of information contained in these "Just Accepted" manuscripts.

ACS Publications

Nano Letters is published by the American Chemical Society. 1155 Sixteenth Street N.W., Washington, DC 20036

Published by American Chemical Society. Copyright © American Chemical Society. However, no copyright claim is made to original U.S. Government works, or works produced by employees of any Commonwealth realm Crown government in the course of their duties.

Impacts of Ion Segregation on Local Optical Properties in Mixed Halide Perovskite Films

Olivia Hentz‡, Zhibo Zhao‡, Silvija Gradečak*

Department of Materials Science and Engineering, Massachusetts Institute of Technology, Cambridge, MA 02139, USA

Abstract

Despite the recent astronomical success of organic-inorganic perovskite solar cells (PSCs), the impact of microscale film inhomogeneities on device performance remains poorly understood. In this work, we study $CH_3NH_3PbI_3$ perovskite films using cathodoluminescence in scanning transmission electron microscopy and show that localized regions with increased cathodoluminescence intensity correspond to iodide-enriched regions. These observations constitute direct evidence that nanoscale stoichiometric variations produce corresponding inhomogeneities in film cathodoluminescence intensity. Moreover, we observe the emergence of high-energy transitions attributed to beam induced iodide segregation, which may mirror the effects of ion migration during PSC operation. Our results demonstrate that such ion segregation can fundamentally change the local optical and microstructural properties of organic-inorganic perovskite films in the course of normal device operation and therefore address the observed complex and unpredictable behavior in PSC devices.

KEYWORDS: Methylammonium-lead halide perovskite, cathodoluminescence, ion migration, optical properties, organic-inorganic perovskite solar cells

Organic-inorganic perovskite solar cells (PSCs) have recently garnered significant interest due to their high efficiencies,[1–3] easy processability,[4] and relatively inexpensive fabrication.[5] Early attention focused on increased device efficiency *via* novel fabrication methods,[6–8] varied architectures,[1,9,10] and material selection,[11–14] but the frequently reported device instability and variability has motivated further research into the fundamental optoelectronic properties of organic-inorganic perovskite materials.[15–18] In particular, maximizing radiative recombination is critical for reaching the thermodynamic efficiency limits of solar cells and other optoelectronic devices,[19] so understanding carrier behavior in organic-inorganic perovskite materials is required for controlled improvement in the stability, reliability, and scalability of organic-inorganic perovskite-based devices. To this end, recent fluorescence microscopy of $CH_3NH_3PbI_3$ films has revealed variations in luminescence intensity between grains and strongly quenched luminescence at grain boundaries, suggesting that trap distribution is likely non-uniform across the film and offering a route to improvement through targeted passivation of these trap states.[20] However, studies thus far have an assumed focus on homogenous, stoichiometric $CH_3NH_3PbI_3$ films without consideration of possible nanoscale variations in local film chemistry.

In this work, we study these local fluctuations using cathodoluminescence in scanning transmission electron microscopy (CL-STEM) in combination with energy dispersive x-ray spectroscopy (EDS), which enabled us to directly correlate local microstructure, composition, and optical properties in the $CH_3NH_3PbI_3$ perovskite film with nanoscale resolution. Our study reveals that spatial luminescence intensity variations are directly related to iodide content fluctuations. Hence, the local stoichiometry of organic-inorganic perovskite films has a measurable impact on radiative carrier recombination. Additionally, localized low-wavelength

spectral features that appear under electron beam illumination in cathodoluminescence in scanning electron microscopy (CL-SEM) and CL-STEM are likely attributable to electron beam-induced iodide segregation. Similar features can arise from ion migration during device operation and may impact device figures of merit including the short circuit current (J_{sc}), open circuit voltage (V_{oc}), and consequently power conversion efficiency.

In this study, we investigated transmission electron microscopy (TEM) samples derived from the same synthesis methods used for high-efficiency PSC devices. Highly efficient PSC devices have been reported with the organic-inorganic perovskite film cast on ZnO (standard device architecture) and PEDOT:PSS (inverted device architecture).[13,21] To mimic these architectures and prepare device-relevant samples for TEM, PEDOT:PSS or ZnO were spin-cast on carbon-supported copper TEM grids followed by spin-casting of a mixture of 1:3 $PbCl_2$:MAI to form the $CH_3NH_3PbI_3$ directly on the grid (Supporting Information, Figure S1). Identical films with a nominal thickness of 350-400 nm were formed on ITO/glass substrates and showed X-ray diffraction characteristic of $CH_3NH_3PbI_3$ as well as strong bandgap photoluminescence centered at 767 nm (Figure 1). Hence, the as-synthesized $CH_3NH_3PbI_3$ films are comparable to those used in high quality device fabrication.

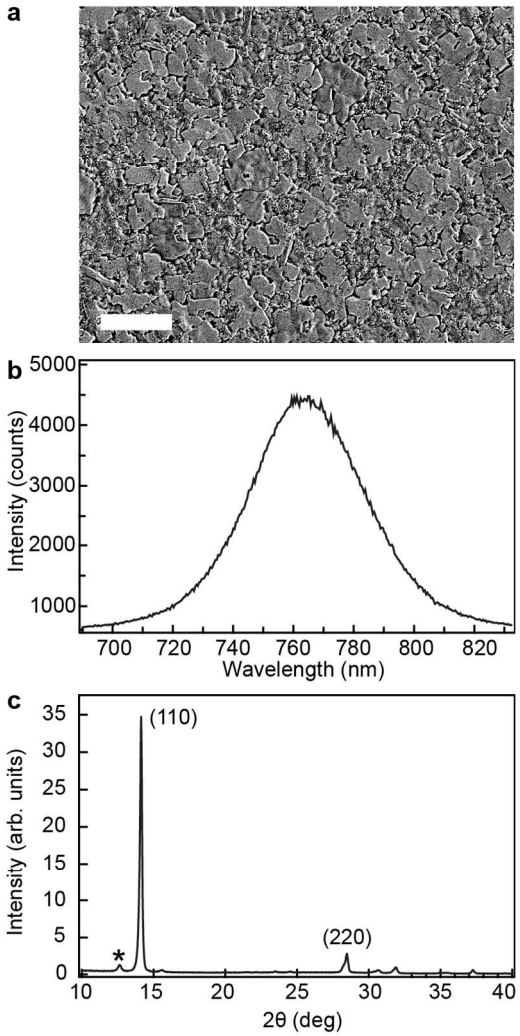

Figure 1. (a) SEM image of $CH_3NH_3PbI_3$ film on PEDOT:PSS on ITO glass. Scale bar is 5 μm. (b) PL and (c) XRD spectra of the perovskite film with (110) and (220) reflections indicated. The asterisk marks trace PbI_2 in the film.

To maximize the CL yield, we first performed low temperature (93 K) panchromatic CL-STEM mapping. CL-STEM measurements were performed at an accelerating voltage of 120 kV on a JEOL 2011 TEM equipped with a Gatan MONOCL3+ cathodoluminescence system, and the sample was cooled using a liquid nitrogen-filled cryo-holder. Panchromatic images were obtained using a photodetector that records the integrated cathodoluminescence intensity irrespective of the emission wavelength. We note here that all CL experiments, unless noted

otherwise, were performed on previously unexposed regions of the sample to minimize possible electron beam-induced artifacts.

CL-STEM images of as-prepared $CH_3NH_3PbI_3$ films show strong spatial variations in luminescence intensity (Figure 2), consistent with previously reported fluorescence microscopy measurements.[20] In contrast to previous studies that attribute variations in luminescence solely to high densities of trap states at surfaces and grain boundaries,[22] we further correlate luminescence intensity with local stoichiometric variations in film chemistry. By directly comparing panchromatic CL maps to their corresponding dark field STEM images in various film regions (Figure 2a,b), it can be observed that highly luminescent areas correspond to regions of darker contrast in dark field STEM (Figure 2c,d). To obtain more direct evidence of the possible relationship between CL and STEM contrast, we recorded multiple CL-STEM intensity line scans in different regions of the sample. A representative result is shown in Figure 2c, and similar line scans from other areas of the sample are provided in the Supporting Information (Supporting Information, Figure S2). All of the results indicate a strong negative correlation between the STEM and CL brightness: high intensity cathodoluminescence corresponds to a drop in the STEM contrast (Figure 2c).

Because the panchromatic CL images were recorded at 93 K, they are representative of the low-temperature phase of the organic-inorganic perovskite material. The transition from the room temperature to the low-temperature phase occurs at 160 K and entails a discontinuous tetragonal-to-orthorhombic change in the symmetry of the unit cell accompanied by a doubling of the unit cell volume.[23] Notably, the stoichiometry of the unit cell in both phases remains constant. To ensure that the observed properties are also present in the room temperature phase

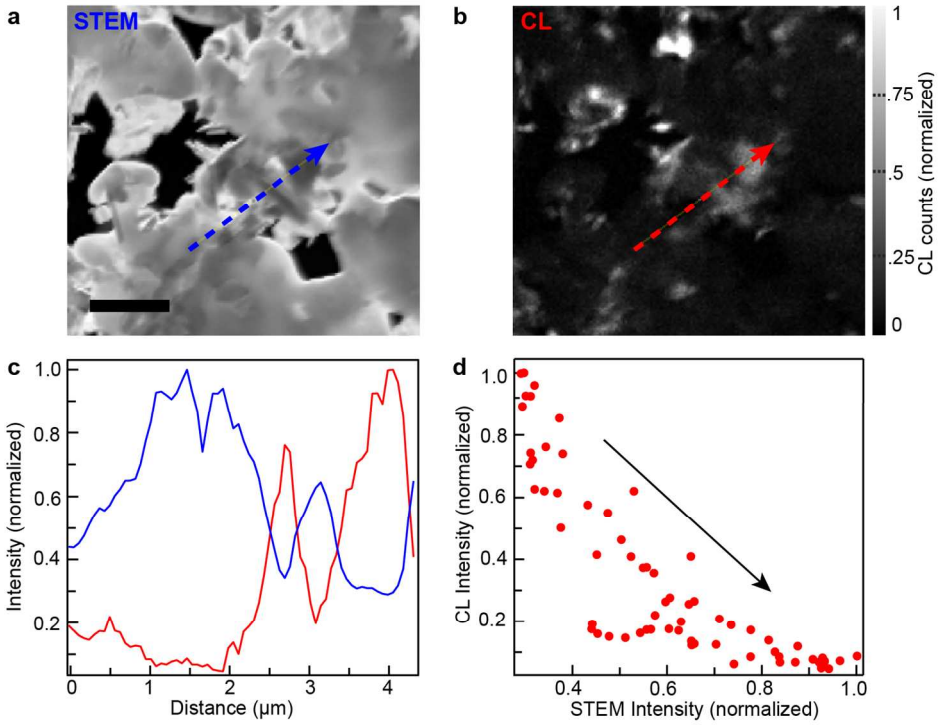

Figure 2. (a) Dark-field STEM image of $CH_3NH_3PbI_3$ film on ZnO and (b) the corresponding panchromatic CL map show luminescence primarily from regions of darker STEM contrast. Scale bar is 2 μm. (c) Intensity STEM (blue) and CL (red) line profiles recorded along the lines shown in (a) and (b). (d) The negative correlation between STEM and CL brightness extracted point-by-point from line scan profiles in (c).

used in PSC devices, we performed room temperature CL measurements on the same samples, and these qualitatively show the same CL-STEM anti-correlation (Supporting Information, Figure S3). Hence, the observed properties are characteristic of the $CH_3NH_3PbI_3$ film and not specific to its low-temperature phase or low-temperature carrier behavior.

The origin of contrast in dark field STEM images is primarily due to mass-thickness variations—areas that are thicker and/or have higher average atomic number (Z) appear brighter due to strong electron scattering. To avoid any thickness-variation effects and focus on the chemical origin of the contrast in dark field STEM images, we performed EDS measurements on areas of the sample that were uniform in thickness. EDS measurements were performed at room temperature in a JEOL 2010F field emission TEM under an accelerating voltage of 200 kV. As

in the case of CL, all EDS scans were acquired on previously unexposed regions of the sample to minimize possible beam-induced artifacts.

Using EDS, we measured the relative iodide content, defined as the fraction of iodide counts among iodide and lead counts, across different regions in these films. (As defined, this value does not directly translate into the absolute atomic fraction of iodide.) EDS spectra show strong signal from iodide and lead, but the residual chloride signal was not detectable (Supporting Information, Figure S4), in agreement with reports that most of the chloride is driven out of the film during the annealing step.[24] We therefore did not include chloride in our quantification of the film composition.

As shown in Figure 3a, point spectra taken in selected regions show increased iodide content in areas of darker STEM contrast, in agreement with expectations based on Z-contrast. Although the cross-sectional SEM imaging performed on a representative region of interest yielded a measured sample thickness between 150-300 nm, the exact sample thickness in the areas investigated using EDS was not known, so the iodide quantification cannot be considered exact. To address this uncertainty, the nominal atomic percent iodide was recalculated at the aforementioned points in Figure 3a assuming a highly conservative range of sample thicknesses between 150-600 nm. Across this entire thickness range, the iodide content was consistently higher at the point of darker contrast with possible quantification uncertainty within 0.5 at. % (s.d.), re-emphasizing the conclusion that the compositional Z-contrast remains the dominant contrast mechanism in the region of interest. To corroborate these point scans, EDS line scans were also obtained to compare relative changes in iodide fraction with corresponding variations in STEM contrast. As shown in Figures 3b and 3c, a line scan across a representative region of interest exhibits a strong negative correlation between the STEM intensity and the relative iodide

content. Other regions show similar behavior and reinforce the negative correlation between dark field STEM contrast and iodide content (Supporting Information, Figure S5). We note here that there may be compositional variations in the z-direction, i.e. through the thickness of the sample, in addition to the observed lateral variations. However, since the electron beam interacts with the entire thickness of the sample, the mass contrast in the z-direction cannot be captured in EDS. Nonetheless, the anti-correlation between STEM contrast and lateral variations in iodide content remains strong.

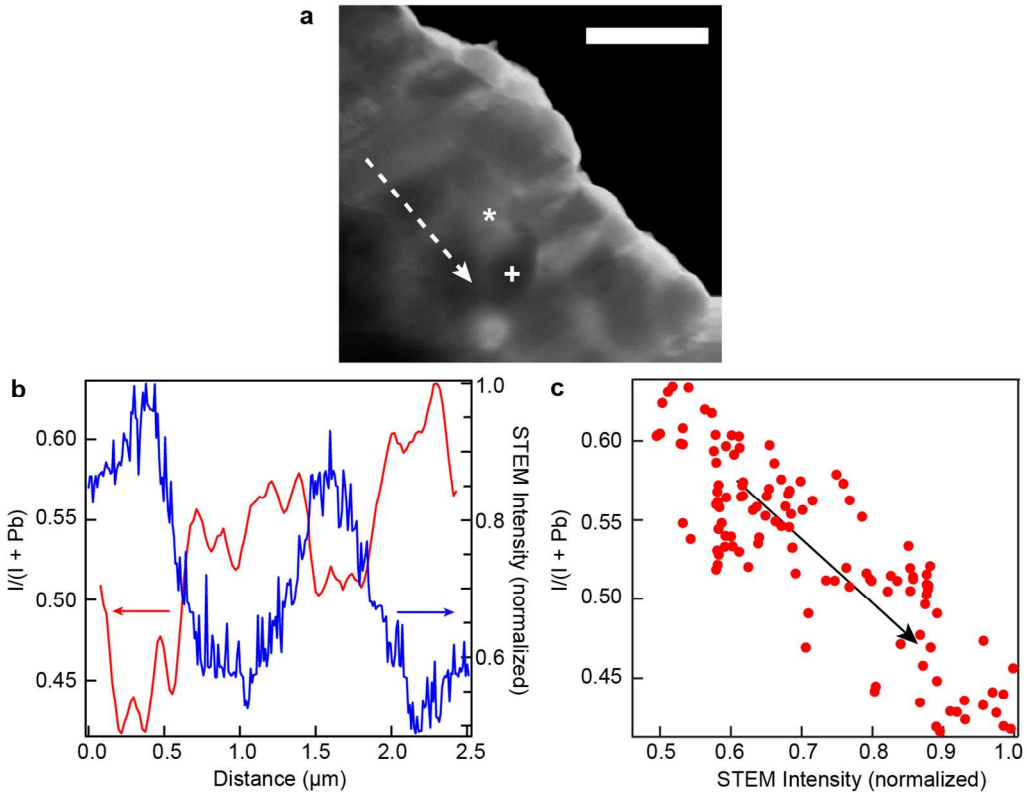

Figure 3. (a) Dark field STEM image of $CH_3NH_3PbI_3$ on PEDOT:PSS with white arrow indicating location of the EDS line scan represented in (b). Accounting for only iodine and lead, positions labeled with (*) and (+) have iodine atomic fraction of 0.802 and 0.835, respectively. Scale bar is 2 μm. (b) EDS line scan tracking the fraction by counts of iodide relative to the combined counts of iodide and lead (Gaussian smoothing applied), plotted as a function of the STEM intensity along this line. (c) Relative fraction of iodide counts *vs*. STEM intensity at points along the line scan revealing a negative correlation.

Taken together, these EDS and CL results show that areas with the strongest luminescence in CL measurements have the highest iodide content. With strong iodide segregation, either increased iodide enhances emission or defects associated with iodide deficiencies strongly quench emission. In either case, it can be concluded that stoichiometric variations, such as those resulting from ion migration/segregation, have a strong impact on the optical properties of these films and, by extension, PSC device performance.

To further address the origin of the spatial non-uniformity observed in the CL intensity maps, we next investigated the spectral characteristics of these perovskite films. Figures 4a-c show the low temperature (93 K) CL spectrum, bright field STEM micrograph, and low temperature panchromatic CL image of the same region of a representative perovskite film. The CL spectrum from the region (Figure 4a) shows two peaks centered at 730 nm and 593 nm. Monochromatic CL images taken at 730 nm and 585 nm (Figure 4d,e) show that the longer wavelength emission is spatially extended over the entire area of the film, while the shorter wavelength emission is highly localized. To study these spectral inhomogeneities in more detail, CL spectra were taken from multiple regions in a number of films, showing three general peak center locations: 585-600 nm, 640-650 nm, and 730-740 nm (Supporting Information, Figure S6). The longest wavelength emission is consistently delocalized, and we therefore attribute this 730-740 nm emission to the intrinsic bandgap emission of the low temperature orthorhombic phase of the perovskite film,[23] analogous to the room temperature phase bandgap emission at 767 nm measured by PL (Figure 1b).

On the other hand, the emergence of shorter wavelength transitions in the spectrum has not, to our knowledge, been previously reported in artifact-free $CH_3NH_3PbI_3$ films. Room temperature CL measurements also exhibit these spectral features, albeit less pronounced, so

such behavior is not specific to the low temperature phase (Supporting Information, Figure S7). The relative prominence of these spectral features at low temperatures suggests they are unlikely to be an artifact of local electron beam-induced heating.[25] Furthermore, their emergence is not specific to samples prepared directly on TEM grids: continuous perovskite films prepared on ITO/glass substrates (in the same way as they would be prepared for devices) and mechanically transferred onto copper TEM grids showed similar spectral characteristics to perovskite films

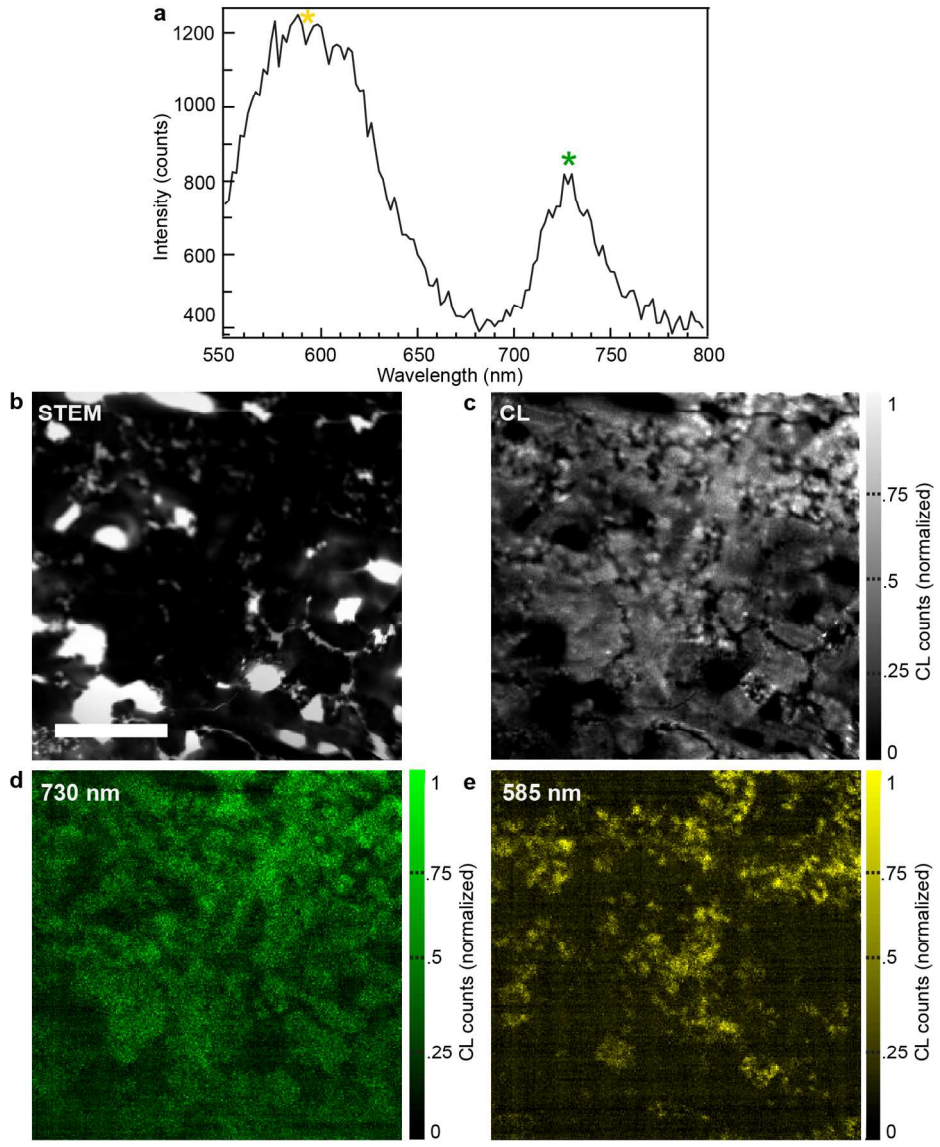

Figure 4. (a) CL spectrum obtained from $CH_3NH_3PbI_3$ film (on ZnO) region shown in the bright field STEM image (b) and the corresponding panchromatic CL map (c). Monochromatic CL

images taken at (d) 730 nm and (e) 585 nm marked in (a) reveal two distinct emission characteristics—a diffuse long wavelength emission and a highly localized shorter wavelength emission. Scale bar is 10 μm.

deposited directly onto TEM grids (Supporting Information, Figure S8). Hence, these spectral inhomogeneities do not represent any temperature or synthesis-induced artifacts and the lower wavelength emissions can likely be attributed to structural changes in the film induced by the electron beam.

To study the effects of electron beam illumination, a $CH_3NH_3PbI_3$ film spun on ZnO/ITO/glass was investigated using CL-SEM. CL-SEM measurements were recorded at 5 kV accelerating voltage and 2 nA beam current using a JEOL-JXA-8200 Superprobe SEM equipped with a cathodoluminescence attachment. The $CH_3NH_3PbI_3$ film was exposed to a scanning electron probe (5 kV, 2 nA) at room temperature while collecting CL spectra at 5 s intervals. In CL-SEM, the 2 nA beam current was rastered over an area of 720 μm^2, yielding an electron dosage of 8.34 C/cm^2 over 30 s. During PSC device operation, a typical current density of ~20 mA/cm^2 corresponds to an electron dosage of 600 C/cm^2 over 30 s, almost two orders of magnitude higher than the electron beam, so any beam-induced structural changes may well be mirrored during device operation.

The spectral time series shown in Figure 5 reveals a clear change in the emission characteristics of the film upon extended exposure to the electron beam. In particular, the longest wavelength emission initially centered at 767 nm quenches and shifts by ~10 nm over the course of 255 s, whereas a lower wavelength emission emerges after approximately 30 s, increases in intensity, and blue-shifts to 660 nm. A CL-STEM spectral time series shows similarly continuous changes in the relative positions and intensities of the high energy and bandgap emission peaks (Supporting Information, Figure S9). The continuous shifts in the peak

wavelengths and intensities suggest corresponding continuous changes in the structural characteristics of the organic-inorganic perovskite film. Due to the low activation energy for the formation and migration of iodide-related defects in these perovskite films,[26] we propose that the observed spectral inhomogeneities result from electron beam-activated migration and formation of iodide vacancies and/or interstitials. The subsequent iodide redistribution creates iodide-enriched and iodide-deficient regions that give rise to local high-energy emissions in the $CH_3NH_3PbI_3$ film observed in our CL-STEM experiments.

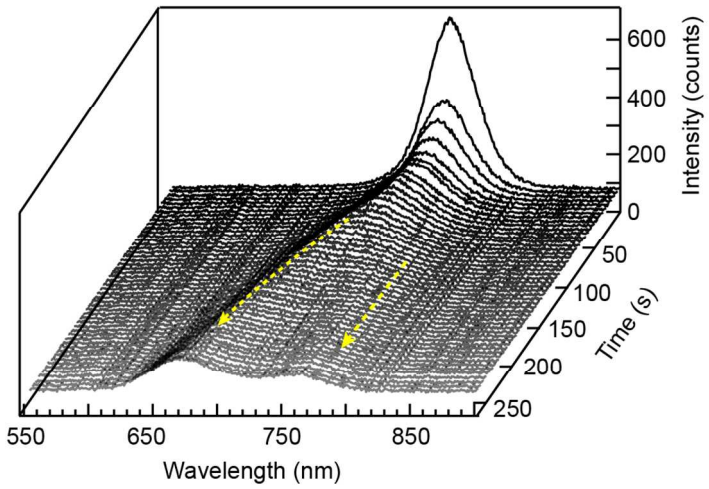

Figure 5. Time evolution of SEM CL spectra of $CH_3NH_3PbI_3$ films on ZnO/ITO/glass taken in 5 s time intervals over 255 s. As indicated by the yellow arrows, the CL emission from the perovskite band gap quenches and shows a slight blue shift with beam exposure (5 kV, 2 nA), while another high-energy (lower wavelength) peak appears and blue shifts. Spectra are offset as a function of exposure time.

Based on the positive correlation between iodide content and luminescence intensity, it is likely that these strong, localized lower wavelength emissions originate from iodide-rich regions of the film. There are several possible mechanisms for local bandgap changes linked to iodide content and bonding characteristics. It has been shown that strain on the perovskite crystal structure can result in band gap changes of the magnitude observed here,[27] and in the case of enhanced iodide segregation, iodide accumulation could cause strain in localized regions of the

material. Changes in the Pb-I-Pb bond angle, which could also potentially result from iodide accumulation producing distortions in the lattice, can also cause such band gap widening.[28] Finally, it is possible that the material undergoes local non-stoichiometric transformation as a result of increased iodide content in specific regions of the film. Though further studies are required to ascertain which of these mechanisms are at work in our regions of interest, the correlation between relative iodide content and CL inhomogeneities suggests that a structural redistribution of iodide has a noticeable effect on both spatial and spectral luminescence characteristics.

It is well-studied that under device operation ion migration results in local compositional variations in organic-inorganic perovskite materials,[26,29] and these variations have been tied to anomalous effects in devices, such as hysteresis under current-voltage measurements.[30] In this study, we expand the understanding of ion migration to show its effect on optical properties in the material, including a potential shift in the band edge as well as the introduction of localized regions of large band gap material under current densities comparable to device operation conditions. Our results could significantly affect both design and analysis of device operation, given that the expected absorption and V_{oc} may be meaningfully altered in these conditions. The emergence of wide bandgap regions could create significant band bending effects that affect both the V_{oc} and charge transport. More work will be needed to elucidate the practical effect of these phenomena; such investigations could potentially help explain the outstanding performance of PSCs.

In conclusion, local stoichiometric variations in iodide content have a significant impact on luminescence and, therefore, carrier properties in $CH_3NH_3PbI_3$ films. In particular, strongly luminescent areas of the organic-inorganic perovskite film correlate with iodide-enriched

regions. Furthermore, these iodide-enriched regions are likely to exhibit inhomogeneous spectral characteristics such as emission at energies higher than the bandgap. Given the ease of iodide-related defect formation and migration in these organic-inorganic perovskite materials, it is likely that these inhomogeneities arise from electron beam-activated iodide segregation and can be extended to structurally similar organic-inorganic perovskite films. It is plausible that similar ion redistribution may occur during normal device operation. Hence, our results strongly suggest that iodide migration/segregation has a distinct effect on film carrier properties that should be taken into account in the context of device performance and consistency. Continued investigation of the effect of ion migration within these films on their optical properties will inform the development and improve the consistency of future PSCs.

ASSOCIATED CONTENT

Supporting Information. Experimental details, SEM of grids used in TEM, Additional STEM and CL-STEM images and line scans at low temperature and room temperature, EDS spectrum, Additional EDS and STEM line scan, Additional CL spectra at low temperature and room temperature, CL spectrum of flakes of $CH_3NH_3PbI_3$ film. This material is available free of charge via the Internet at http://pubs.acs.org.

AUTHOR INFORMATION

Corresponding Author

*Email: gradecak@mit.edu

‡These authors contributed equally.

The authors declare no competing financial interests.

ACKNOWLEDGMENTS

This work was supported by the Center for Excitonics, an Energy Frontier Research Center funded by the U.S. Department of Energy, Office of Science, Office of Basic Energy Sciences, under Award Number DE-SC0001088. O.H. and Z.Z. acknowledge graduate fellowship support through the National Science Foundation Graduate Research Fellowship under Grant No. 1122374. This work made use of the MRSEC Shared Experimental Facilities at MIT, supported by the National Science Foundation under award number DMR-1419807. Any opinion, findings, and conclusions or recommendations expressed in this material are those of the authors and do not necessarily reflect the views of the National Science Foundation. The authors also thank Dr. N. Chatterjee for training and access to CL-SEM facilities.

REFERENCES:

(1) Correa Baena, J. P.; Steier, L.; Tress, W.; Saliba, M.; Neutzner, S.; Matsui, T.; Giordano, F.; Jacobsson, T. J.; Kandada, A. R. S.; Zakeeruddin, S. M.; Petrozza, A.; Abate, A.; Nazeeruddin, M. K.; Grätzel, M.; Hagfeldt, A. *Energy Environ. Sci.* **2015**, *8***,** 2928–2934.

(2) Jeon, N. J.; Noh, J. H.; Yang, W. S.; Kim, Y. C.; Ryu, S.; Seo, J.; Seok, S. I. *Nature* **2015**, *517***,** 476–480.

(3) Yang, W. S.; Noh, J. H.; Jeon, N. J.; Kim, Y. C.; Ryu, S.; Seo, J.; Seok, S. I. *Science* **2015**, *348***,** 1234–1237.

(4) You, J.; Hong, Z.; Yang, Y.; Chen, Q.; Cai, M.; Song, T.-B.; Chen, C.-C.; Lu, S.; Liu, Y.; Zhou, H.; Yang, Y. *ACS Nano* **2014**, *8*, 1674–1680.

(5) Snaith, H. J. *J. Phys. Chem. Lett* **2013**, *4*, 3623−3630.

(6) Burschka, J.; Pellet, N.; Moon, S.-J.; Humphry-Baker, R.; Gao, P.; Nazeeruddin, M. K.; Grätzel, M. *Nature* **2013**, *499*, 316–319.

(7) Chen, Q.; Zhou, H.; Hong, Z.; Luo, S.; Duan, H.-S.; Wang, H.-H.; Liu, Y.; Li, G.; Yang. Y. *J. Am. Chem. Soc.* **2013**, *136*, 622-625.

(8) Nie, W.; Tsai, H.; Asadpour, R.; Blancon, J.-C.; Neukirch, A. J.; Gupta, G.; Crochet, J. J.; Chhowalla, M.; Tretiak, S.; Alam, M. A.; Wang, H.-L.; Mohite, A. D. *Science* **2015**, *347*, 522–525.

(9) Lee, M. M.; Teuscher, J.; Miyasaka, T.; Murakami, T. N.; Snaith, H. J. *Science* **2012**, *338*, 643–647.

(10) Son, D. Y.; Im, J. H.; Kim, H. S.; Park, N. G. *J. Phys. Chem. C* **2014**, *118*, 16567–16573.

(11) Christians, J. A.; Fung, R. C. M.; Kamat, P. V. *J. Am. Chem. Soc.* **2014**, *136*, 758–764.

(12) Hao, F.; Stoumpos, C. C.; Cao, D. H.; Chang, R. P. H.; Kanatzidis, M. G. *Nat. Photonics* **2014**, *8*, 489–494.

(13) Malinkiewicz, O.; Yella, A.; Lee, Y. H.; Espallargas, G. M.; Graetzel, M.; Nazeeruddin, M. K.; Bolink, H. J. *Nat. Photonics* **2013**, *8*, 128-132.

(14) Suarez, B.; Gonzalez-Pedro, V.; Ripolles, T. S.; Sanchez, R. S.; Otero, L.; Mora-Sero, I. *J. Phys. Chem. Lett.* **2014**, *5*, 1628–1635.

(15) Edri, E.; Kirmayer, S.; Mukhopadhyay, S.; Gartsman, K; Hodes, G.; Cahen, D. *Nat. Commun.* **2014**, *5*, 3461.

(16) Marchioro, A.; Teuscher, J.; Friedrich, D.; Kunst, M.; van de Krol, R.; Moehl, T.; Grätzel, M.; Moser, J.-E. *Nat. Photonics* **2014**, *8*, 250–255.

(17) Mosconi, E.; Amat, A.; Nazeeruddin, K.; Grätzel, M.; De Angelis, F. *J. Phys. Chem. C* **2013**, *117*, 13902–13913.

(18) Ponseca, C.S.; Savenjie, T. J.; Abdellah, M.; Zheng, K.; Yartsev, A.; Pascher, T.; Harlang, T.; Chabera, P.; Pullerits, T.; Stepanov, A.; Wolf, J. P.; Sundström, V. *J. Phys. Chem. Soc.* **2014**, *136*, 5189-5192.

(19) Miller, O.D.; Yablonovitch, E.; Kurtz, S.R. *IEEE J. Photovolt.* **2012**, *2*, 303-311.

(20) de Quilettes, D. W.; Vorpahl, S. M.; Stranks, S. D.; Nagaoka, H.; Eperon, G. E.; Ziffer, M. E.; Snaith, H. J.; Ginger, D. S. *Science* **2015**, *348*, 683–686.

(21) Liu, D.; Kelly, T. L. *Nat. Photonics* 2013, *8*, 133–138.

(22) Bischak, C. G., Sanehira, E. M., Precht, J. T., Luther, J. M., & Ginsberg, N. S. *Nano Lett.* 2015, 15, 4799-4807.

(23) Wehrenfennig, C.; Liu, M.; Snaith, H. J.; Johnston, M. B.; Herz, L. M. *APL Mat.* **2014**, *2*, 081513.

(24) Colella, S.; Mosconi, E.; Fedeli, P.; Listorti, A.; Gazza, F.; Orlandi, F.; Ferro, P.; Besagni, T.; Rizzo, A.; Calestani, G.; Gigli, G.; De Angelis, F.; Mosca, R. *Chem. Mater.* **2013**, *25*, 4613–4618.

(25) Xiao, C.; Li, Z.; Guthrey, H.; Moseley, J.; Yang, Y.; Wozny, S.; Moutinho, H.; To, B.; Berry, J. J.; Gorman, B.; Yan, Y.; Zhu, K.; Al-Jassim, M. *J. Phys. Chem. C*, **2015**, *119*, 26904-26911.

(26) Azpiroz, J. M.; Mosconi, E.; Bisquert, J.; De Angelis, F. *Energy Environ. Sci.* **2015**, *8*, 2118-2127.

(27) Grote, C.; Berger, R. F. *J. Phys. Chem. C* **2015**, *119*, 22832-22837.

(28) Filip, M. R.; Eperon, G. E.; Snaith, H. J.; Giustino, F. *Nat. Commun.* **2014**, *5*, 5757.

(29) Haruyama, J.; Sodeyama, K.; Han, L.; Tateyama, Y. *J. Am. Chem. Soc.* **2015**, *137*, 10048-10051.

(30) Tress, W.; Marinova, N.; Moehl, T.; Zakeeruddin, S. M.; Nazeeruddin, M. K.; Grätzel, M. *Energy Environ. Sci.* **2015**, *8*, 995–1004.

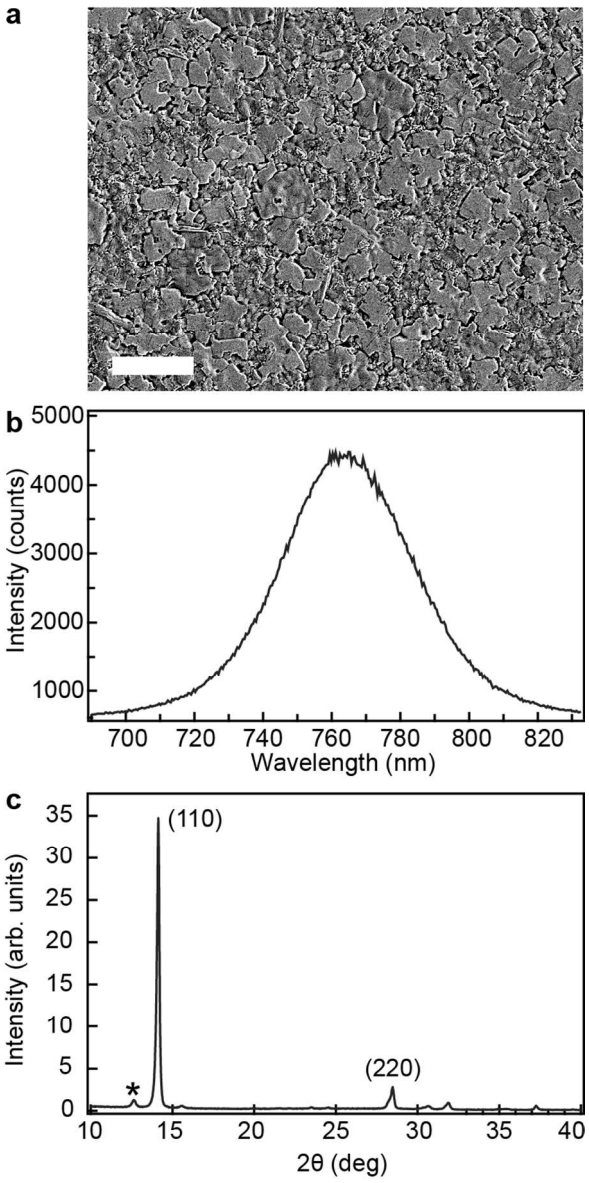

Figure 1
69x139mm (300 x 300 DPI)

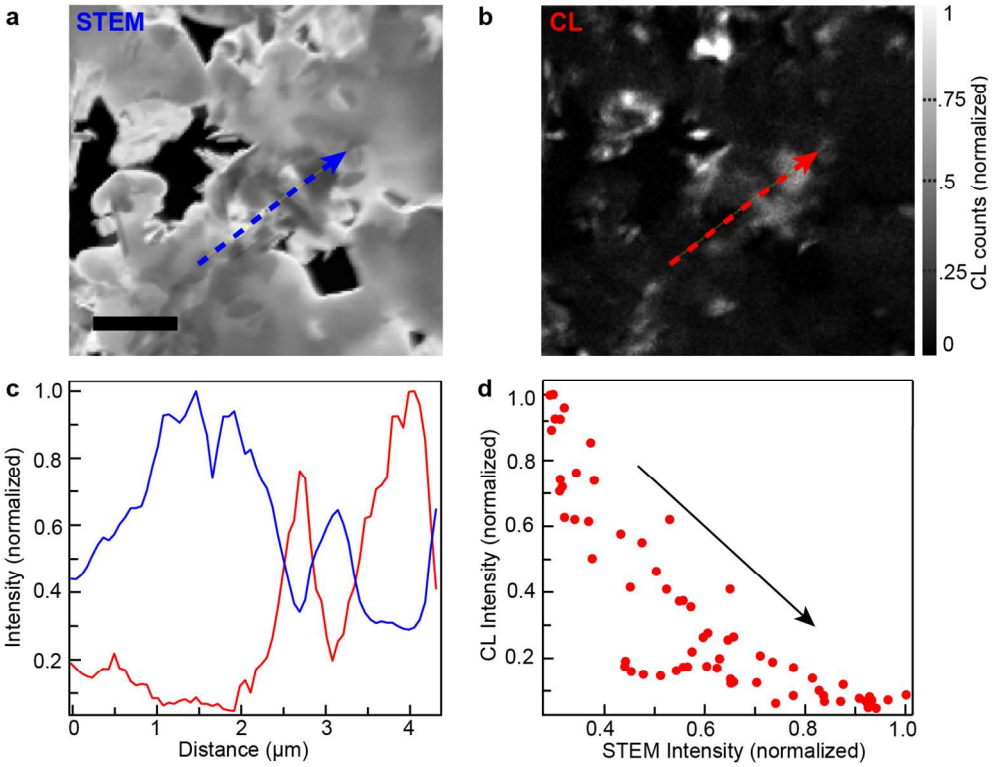

Figure 2
135x104mm (300 x 300 DPI)

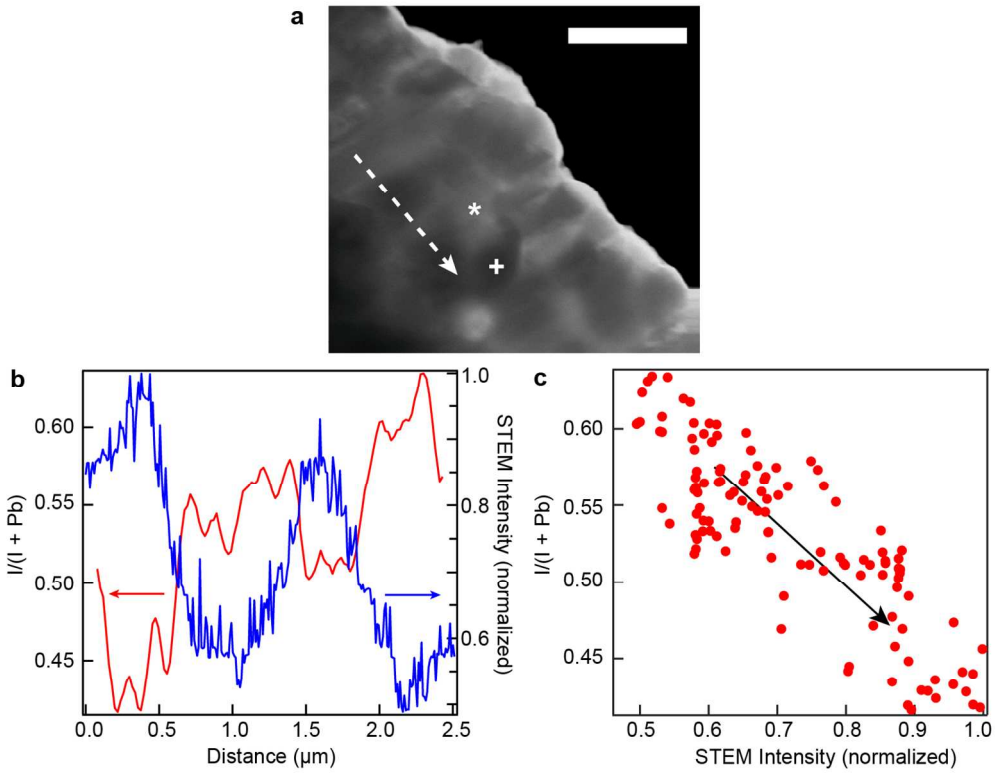

Figure 3
136x106mm (300 x 300 DPI)

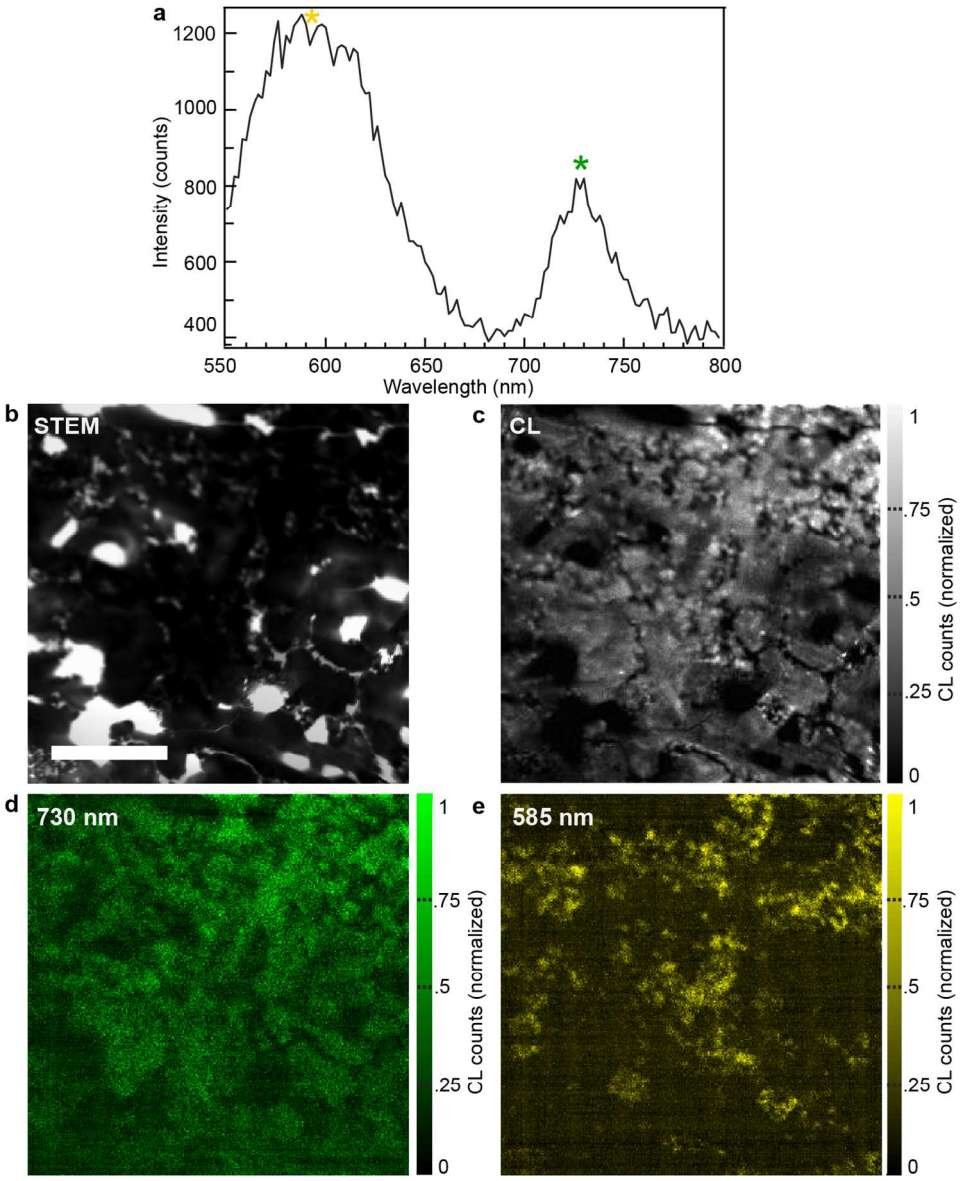

Figure 4
137x170mm (300 x 300 DPI)

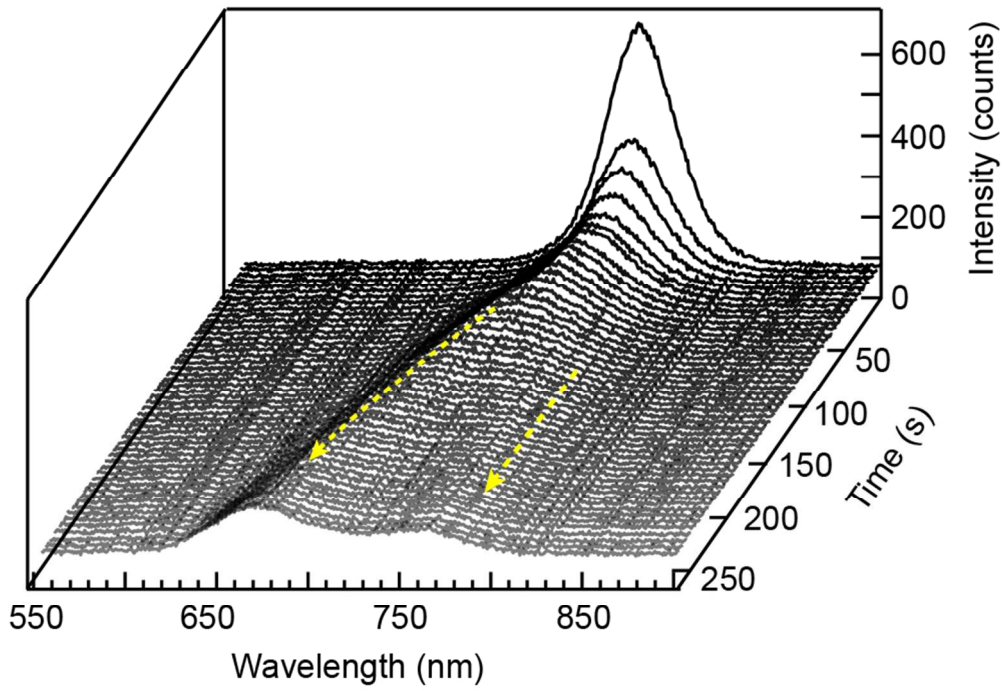

Figure 5
84x63mm (300 x 300 DPI)

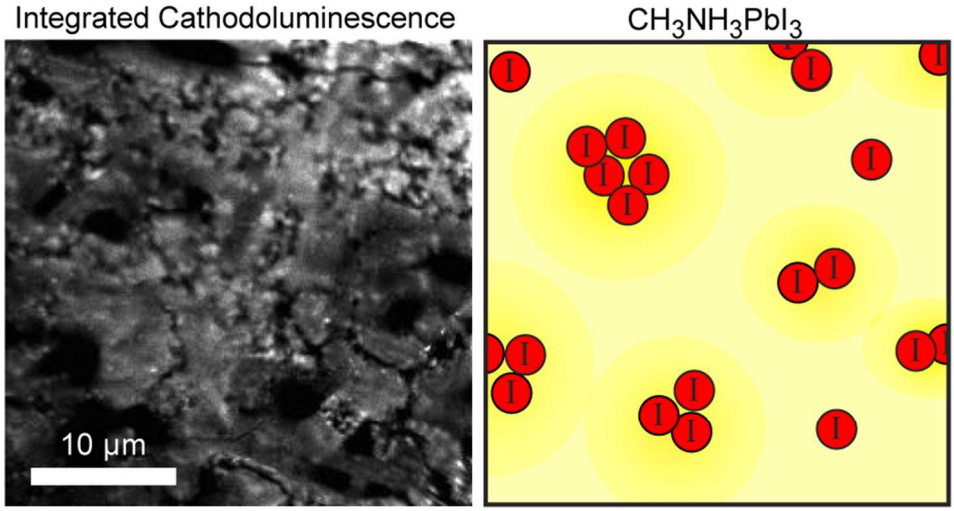

TOC
82x43mm (300 x 300 DPI)